Journal of Materials Chemistry C

ROYAL SOCIETY OF CHEMISTRY

COMMUNICATION

View Article Online
View Journal | View Issue

Cite this: J. Mater. Chem. C, 2021, 9, 7888

Received 21st April 2021,
Accepted 9th June 2021

DOI: 10.1039/d1tc01837j

rsc.li/materials-c

Fabrication of a γ-In_2Se_3/Si heterostructure phototransistor for heart rate detection†

Yue Zhang,[a] Ming Wang,[a] Kaijun Cao,[a] Chunyan Wu, *[a] Chao Xie,[b] Yuxue Zhou[c] and Linbao Luo *[a]

A γ-In_2Se_3/Si heterostructure phototransistor with a broadened photoresponse has been developed, presenting a responsivity, specific detectivity and response speed of 10.24 A W^{-1}, 8.63 × 10^{12} Jones and 0.76/0.85 ms (rise time/fall time) at 450 nm, respectively. The high responsivity could be attributed to the depressed dark current of the γ-In_2Se_3 nanofilm and the high gain arising from the gating effect of the phototransistor. Further analysis reveals that the relatively high responsivity and fast response speed facilitate the application of the device in real-time and accurate health monitoring, such as heart rate detection.

Like many other nontransition metal chalcogenides, indium(III) selenide (In_2Se_3) exhibits intricate polymorphism and complex phase transition. There are five commonly identified crystalline forms of In_2Se_3: layer-structured α-phase, β-phase and κ-phase (formed by inserting a cationic vacancy plane every three in-layers along the *ab*-direction), defect wurtzite γ-phase and high-temperature δ-phase.[1] The phase-dependent properties of In_2Se_3 have been extensively exploited and it shows attractive applications in multiple fields including photovoltaic solar cells, nonvolatile phase change memories and ion batteries.[2–4] What is more, In_2Se_3 has been regarded as one of the most promising materials for high-performance photodetectors due to its direct band gap, high absorption coefficient and high sensitivity.[5,6] For instance, Zhai *et al.* first investigated the photoconductive characteristics of a high-quality In_2Se_3 individual nanowire, which shows a high responsivity of 89 A W^{-1} at 500 nm.[7] Yu *et al.* developed a UV-vis-NIR photodetector based on exfoliated α-In_2Se_3 nanosheets, presenting a high responsivity of 395 A W^{-1} and fast response of 18 ms at 300 nm.[8] High-quality monolayered α-In_2Se_3 synthesized through the process of thermal evaporation also shows good photoresponsivity of 340 A W^{-1} as well as 6/12 ms for the rise/fall time at 532 nm.[9] The high photosensitivity and fast photoresponse are ascribed to the high quality of the single crystal and its large surface-to-volume ratio. However, the synthesis of high-quality In_2Se_3 nanostructures still remains to be a challenge. The intrinsic defects or the native surface oxides commonly existing in the nanostructures may function as long-lived trap states, leading to a high gain based on the photoconductive effect but at the expense of response time (even up to 9 s).[10,11] What is more, the limited size of the obtained nanosheets/nanoflakes inevitably hinders the large-scale fabrication of the devices.[12]

Physical vapor deposition such as radio frequency (RF) magnetron sputtering[13] and pulsed laser deposition (PLD)[14] provides an efficient and low-cost method for the large-scale fabrication of In_2Se_3 film. However, the as-prepared In_2Se_3 film still suffers from the lowered conductivity arising from the existence of grain boundaries in the polycrystalline film. Efforts are still needed to improve the performance of In_2Se_3 film-based photodetectors. Herein, we report the development of a high-performance γ-In_2Se_3/Si heterostructure phototransistor. With the help of the gate effect of the transistor, a broadened photoresponse over the range of 365–970 nm has been achieved, presenting responsivity and specific detectivity of 10.24 A W^{-1} and 8.63 × 10^{12} Jones at 450 nm, respectively, as well as a fast response speed (0.76/0.85 ms for rise time τ_r/fall time τ_f). What is more, the device is capable of accurately detecting heart rate (HR) with satisfactory reliability, suggesting the potential application in real-time health monitoring.

The detailed schematic process for fabricating the In_2Se_3/Si heterostructure phototransistor is shown in Fig. S1 (ESI†) and Fig. 1a. Typically, a pre-cleaned lightly doped n-type Si (resistivity of ~1–10 Ω cm)/SiO_2 (300 nm) substrate was patterned with a rectangular window (channel length: 30 μm, channel width: 500 μm) using photolithography in advance, followed by its immersion in a BOE solution ($HF:NH_4F:H_2O$ = 3 mL : 6 g : 10 mL) for 5 min to remove the SiO_2 layer. Afterwards, a second photolithography process was employed to define a

[a] School of Microelectronics, Hefei University of Technology, Hefei, Anhui 230009, P. R. China. E-mail: cywu@hfut.edu.cn, luolb@hfut.edu.cn
[b] School of Electronics and Information Engineering, Anhui University, Hefei, Anhui 230601, P. R. China
[c] College of Physical Science and Technology, Yangzhou University, Yangzhou, Jiangsu 225002, P. R. China

† Electronic supplementary information (ESI) available. See DOI: 10.1039/d1tc01837j

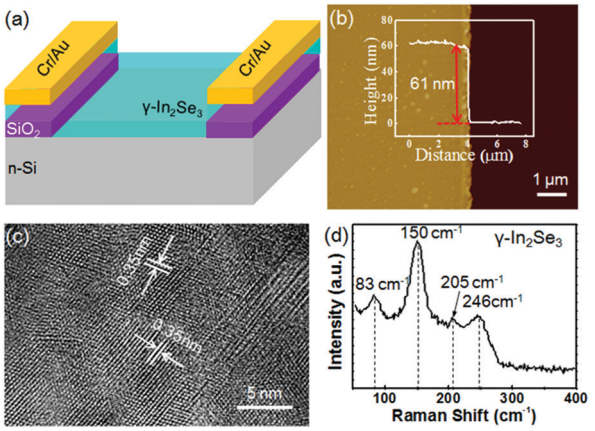

Fig. 1 (a) Schematic illustration of the γ-In_2Se_3/Si heterostructure phototransistor. (b) AFM image of the γ-In_2Se_3 nanofilm on the SiO_2/Si substrate. Inset shows the height profile. (c) HRTEM image and (d) Raman spectrum of the γ-In_2Se_3 nanofilm.

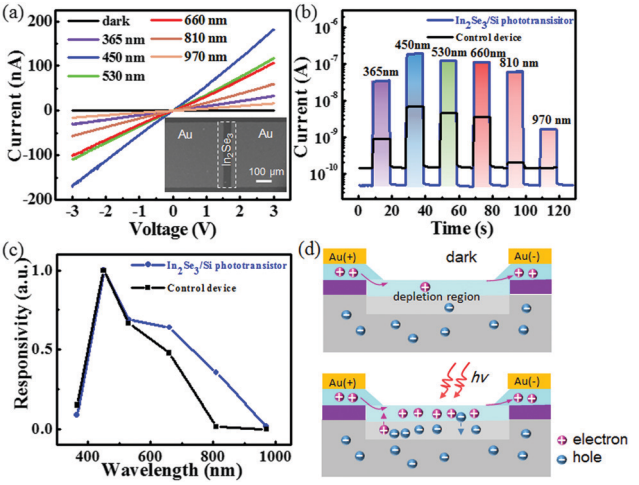

Fig. 2 (a) *I–V* curves of the device in the dark and upon light illumination with different wavelengths at a fixed light intensity (3.06 mW cm^{-2}). (b) Time-dependent photoresponse and (c) normalized spectral response of the γ-In_2Se_3/Si phototransistor and the control device at 3 V bias. (d) Working mechanism of the γ-In_2Se_3/Si phototransistor in the dark and upon light illumination.

larger window size for the deposition of the γ-In_2Se_3 nanofilm onto the exposed Si wafer, which was accomplished *via* RF magnetron sputtering.[13] 10 nm Cr/50 nm Au bilayer metal electrode pairs with the channel length of 50 μm were deposited onto the γ-In_2Se_3 film through electron beam evaporation. A control device without an etched Si window was also assembled for comparison. The atomic force microscopy (AFM) image reveals that the nanofilm has a relatively smooth surface with a root mean square roughness of about 1.8 nm (shown in Fig. 1b). The thickness of the nanofilm is determined to be 61 nm by the inset height profile. Fig. 1c displays the high resolution transmission electron microscopy (HRTEM) image of the nanofilm. Well-defined 2D lattice fringes can be observed, verifying the good crystallinity of the obtained nanofilm. The inter-planar spacings of 0.35 nm correspond to the (110) crystal plane of hexagonal γ-In_2Se_3 (JCPDS no. 40–1407). Furthermore, the Raman spectrum (Fig. 1d) is well consistent with the previously reported γ-In_2Se_3.[13]

Fig. 2a plots the current–voltage (*I–V*) curves of the device measured in the dark and upon light illumination with different wavelengths (365 nm–970 nm) at a fixed light intensity (3.06 mW cm^{-2}). Apparently, the device shows a pronounced photoresponse to all illumination cases. The photocurrent at 3 V bias reaches a maximum 191 nA upon 450 nm illumination and then decreases with the increase of the incident light wavelength. The time-dependent photoresponse shown in Fig. 2b reveals that the dark current of the device slightly decreases and the photocurrent dramatically increases by one order of magnitude when compared to the control device. This can be understood by the working mechanism of the In_2Se_3/Si heterostructure photodetector in the dark and upon light illumination shown in Fig. S2 (ESI†) and Fig. 2d. When the *p*-type γ-In_2Se_3 nanofilm is in contact with the n-type Si, electrons (holes) will move from Si (γ-In_2Se_3) to γ-In_2Se_3 (Si) until their Fermi levels are aligned at the same energy level, producing a built-in electric field (a depletion region) with the direction from *n*-Si to γ-In_2Se_3 at the interface. The majority of carriers (holes) in the γ-In_2Se_3 channel layer are depleted, leading to a lower dark current. While upon light illumination with the photon energy, which is higher than that of the bandgap of γ-In_2Se_3 or Si, the photogenerated carriers within or near the depletion region would be rapidly separated toward the opposite directions in the presence of the built-in electric field. The electrons would be swept into Si and get trapped there, acting as a local gate to effectively modulate the conductivity of the γ-In_2Se_3 layer through capacitive coupling.[15] On the contrary, the holes would be swept into the γ-In_2Se_3 channel layer. Due to the spatial separation, the recombination of photogenerated electrons and holes is greatly suppressed. Therefore, driven by the external bias, the holes in the γ-In_2Se_3 channel layer would be transported fast and recirculate multiple times before recombination, giving rise to a higher electrical gain.[16,17] For quantitative assessment of the device performance, responsivity (R) is calculated according to the equation $R = \frac{I_{light} - I_{dark}}{SP_{in}}$ and the wavelength-dependent normalized responsivity of both the In_2Se_3/Si phototransistor and the control device at 3 V bias are plotted in Fig. 2c.[18] Clearly, the γ-In_2Se_3/Si phototransistor presents a broadened photoresponse than the control device, especially in the wavelength range beyond the absorption limit of intrinsic γ-In_2Se_3 (~590 nm). This also verifies the contribution of Si to the enhanced photoresponse.[19]

Fig. 3a presents the photoresponse characteristics of the device under 450 nm illumination with varied light intensity. We can easily find that the current of the device at 3 V bias increases gradually from 15 nA to 220 nA when the light intensity increases from 4 μW cm^{-2} to 3.67 mW cm^{-2}. This can be explained by the increased amount of photoexcited carriers at an elevated light intensity. The stronger illumination will generate more photon-excited electron–hole pairs and

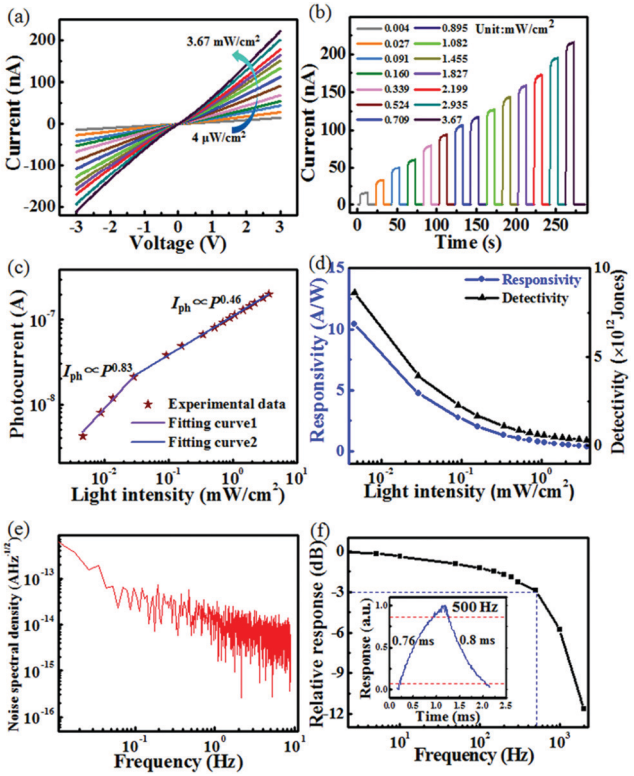

Fig. 3 (a) *I*–*V* curves of the device under 450 nm light illumination with various light intensities. (b) Time-dependent photoresponse at 3 V bias. (c) Photocurrent as a function of light intensity. (d) Responsivity and specific detectivity as a function of light intensity. (e) The noise spectral density as based on the Fourier transform of the dark current. (f) Frequency response of the device. Inset shows the single magnified photoresponse curve at 500 Hz for estimating rise/fall times.

therefore lead to higher current. It should be emphasized that the device can still display a photocurrent of 15 nA even at a weak light intensity of 4 μW cm^{-2}, suggesting the possibility of weak light detection. The time-dependent photoresponse (Fig. 3b) further displays a reproducible photo-switching property with steep rise and fall edges, implying a fast response speed of the device. The photocurrent as a function of light intensity can be expressed as a widely explored power equation: $I_{ph} \propto P^{\theta}$, where I_{ph} is defined as the net photocurrent obtained by subtracting the current measured in the dark from the current measured under light illumination ($I_{ph} = I_{light} - I_{dark}$) and the exponent θ is an empirical value reflecting the recombination of the photocarriers.[20] As plotted in Fig. 3c, θ is fitted to be 0.83 in the relatively low light intensity range (from 4 μW cm^{-2} to 29 μW cm^{-2}) and 0.46 in the high light intensity range (from 29 μW cm^{-2} to 3.67 mW cm^{-2}), respectively. This result suggests the increased recombination activity arising from the higher density of the photoexcited carriers.[21] The responsivity decreases with the increase in the light intensity and reaches 10.24 A W^{-1} under the light intensity of 4 μW cm^{-2} at 3 V, which greatly overpasses the value of the control device (0.27 A W^{-1}), verifying the effect of the built-in electric field. The gain G was calculated to be 28 according to the equation $G = \frac{hcR}{e\lambda}$.[22] The responsivity and gain are relatively lower than those of the In_2Se_3 single crystal based devices,[8,9] which may be ascribed to the increased recombination arising from the grain boundaries or defects in the nanofilm. However, it is comparable to that of the CVD-grown and PLD-grown In_2Se_3 nanofilms (shown in Table S1, ESI†).[14,23] Another key parameter, specific detectivity (D*), can be calculated using the formula of noise equivalent power (NEP):[24] $NEP = \frac{\overline{i_n^2}^{1/2}}{R}$ and $D^* = \frac{(S\Delta f)^{1/2}}{NEP}$, where $\overline{i_n^2}^{1/2}$ is the root mean square value of the noise current and Δf is the specific bandwidth. As shown in Fig. 3e, the noise spectral density of the photodetector was 1.62 × 10^{-14} AHz$^{-1/2}$ at the bandwidth of 1 Hz, which was deduced from the FFT transfer of the dark current (Fig. S3, ESI†).[25] Therefore, the lowest NEP and the highest D^* at 450 nm were calculated to be 1.58 × 10^{-15} WHz$^{-1/2}$ and 8.63 × 10^{12} Jones, respectively, which represents the ability to detect weak optical signals. The transient photoresponse of the device at various frequencies was further researched (Fig. S4, ESI†) and the normalized response as a function of the frequency is shown in Fig. 3f, indicating a −3 dB bandwidth of about 500 kHz. From the single magnified cycle at the frequency of 500 Hz (inset in Fig. 3f), the rise time (τ_r) and the fall time (τ_f) were estimated to be about 0.76 ms and 0.85 ms, respectively. The gain–bandwidth product (GBP = G/τ) of the phototransistor was calculated to be about 4 × 10^4, which was far below the theoretical limit and the value of some reported low-dimensional photodetectors such as Te photodetectors.[26,27] This may also be ascribed to the grain boundaries and defects in the obtained γ-In_2Se_3 nanofilm.

In light of the spectral response covering the characteristic absorption of hemoglobin and the fast response speed of the as-fabricated γ-In_2Se_3/Si phototransistor, we then expand its application to heart rate (HR) detection by photoplethysmography (PPG) test.[28,29] As shown in Fig. 4a and b, the light emitted from the LED transmits through the finger and reaches the γ-In_2Se_3/Si phototransistor. With the change of the blood volume in the veins during the cardiac cycles, pulsatile signals are obtained which can be extracted to evaluate the HR. Fig. 4c presents the pulse PPG signals obtained using the γ-In_2Se_3/Si phototransistor and the control device under 660 nm illumination. Clearly, the PPG signals obtained from the γ-In_2Se_3/Si phototransistor are one order of magnitude stronger than that of the control device, accompanied by a more regular waveform. This should be ascribed to the remarkably improved photoresponse property of the γ-In_2Se_3/Si phototransistor. Fig. 4d presents the digital volume pulse (DVP) of a single cardiac cycle obtained from the PPG signal marked by the dotted square shown in Fig. 4c, in which the systolic and diastolic peaks can be well identified. What is more, the ΔT_{DVP} (the time interval between the systolic peak and later diastolic peak, determined by the artery stiffness) is deduced to be 317 ms, which shows good condition of the arteries and is well consistent with the age of the tested author (26 years).[30] When illuminated using a 530 nm LED, the PPG signals show a less regular waveform, which is caused by the weaker penetrability

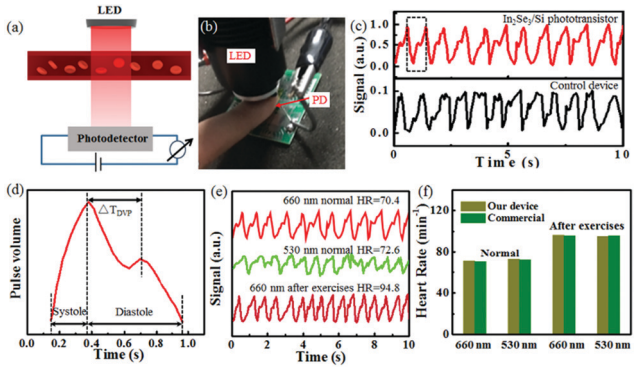

Fig. 4 (a) Schematic diagram and (b) set up of the heart rate detection system. (c) Temporal photocurrent response of the γ-In_2Se_3/Si phototransistor and the control device under 660 nm illumination. (d) The digital volume pulse of a single cardiac cycle. (e) Temporal photocurrent response of the device at normal (under 660 nm and 530 nm illumination) and after-exercise conditions (under 660 nm illumination). (f) Comparison of the detected HR of our detector at different conditions with a commercial Mi band wristband.

of the 530 nm light compared to 660 nm light. By dividing 60 s by the average interbeat interval (IBI) in each case, the HR of the author under normal and after-exercise conditions is determined to be 70.4 and 94.8 beats min^{-1}, respectively, which is well consistent with the measurement results of a commercial Mi band wristband (Fig. 4e, f and Table S2, ESI†). Therefore, the γ-In_2Se_3/Si phototransistor presents potential application for accurate and real-time monitoring of health signals.

In conclusion, a sensitive γ-In_2Se_3/Si heterostructure phototransistor with a broadband photoresponse over the range 365–970 nm and fast response speed has been developed. The dark current was depressed and the photocurrent was dramatically increased, leading to responsivity and specific detectivity values of 10.24 A W^{-1} and 8.63 × 10^{12} Jones, respectively. This relatively good photoresponse along with the fast response speed (0.76/0.85 ms for the rise time/fall time) enables the as-fabricated γ-In_2Se_3/Si phototransistor to be used in real-time health-monitoring, such as heart rate detection. This work provides a facile and effective method for the fabrication of a high-performance nanofilm-based photodetector with good compatibility with an Si-based integrated system.

Conflicts of interest

There are no conflicts to declare.

Acknowledgements

This work was supported by the National Natural Science Foundation of China (NSFC, No. 62074048, 51902078), the Fundamental Research Funds for the Central Universities (No. PA2020GDKC0014, JZ2020HGTB0051, JZ2018HGPB0275, JZ2018HGXC0001), and Anhui Provincial Natural Science Foundation (No. 2008085MF205).

Notes and references

1 L. Liu, J. Y. Dong, J. Q. Huang, A. Nie, K. Zhai, J. Y. Xiang, B. C. Wang, F. S. Wen, C. P. Mu, Z. S. Zhao, Y. J. Gong, Y. J. Tian and Z. Y. Liu, *Chem. Mater.*, 2019, **31**, 10143–10149.
2 J. Wang, H. Yu, C. Hou and J. Zhang, *Sol. RRL*, 2020, **4**, 1900428.
3 D. Kang, T. Rim, C. K. Baek, M. Meyyappan and J. Lee, *Appl. Phys. Lett.*, 2013, **103**, 233504.
4 C. Julien, E. Hatzikraniotis, A. Chevy and K. Kambas, *Mater. Res. Bull.*, 1985, **20**, 287–292.
5 B. Tang, L. Hou, M. Sun, F. Lv, J. Liao, W. Ji and Q. Chen, *Nanoscale*, 2019, **11**, 12817–12828.
6 B. Tang, L. Hou, M. Sun, F. Lv, J. Liao, W. Ji and Q. Chen, *Nanoscale*, 2019, **11**, 12817–12828.
7 T. Zhai, X. Fang, M. Liao, X. Xu, L. Li, B. Liu, Y. Koide, Y. Ma, J. Yao, Y. Bando and D. Golberg, *ACS Nano*, 2010, **4**, 1596–1602.
8 R. B. Jacobs-Gedrim, M. Shanmugam, N. Jain, C. A. Durcan, M. T. Murphy, T. M. Murray, R. J. Matyi, R. L. Moore and B. Yu, *ACS Nano*, 2014, **8**, 514–521.
9 J. Zhou, Q. Zeng, D. Lv, L. Sun, L. Niu, W. Fu, F. Liu, Z. Shen, C. Jin and Z. Liu, *Nano Lett.*, 2015, **15**, 6400–6405.
10 R. K. Mech, S. V. Solanke, N. Mohta, M. Rangarajan and D. N. Nath, *IEEE Photonics Technol. Lett.*, 2019, **31**, 905–908.
11 J. O. Island, S. I. Blanter, M. Buscema, H. S. J. van der Zant and A. Castellanos-Gomez, *Nano Lett.*, 2015, **15**, 7853–7858.
12 M. Lin, D. Wu, Y. Zhou, W. Huang, W. Jiang, W. Zheng, S. Zhao, C. Jin, Y. Guo, H. Peng and Z. Liu, *J. Am. Chem. Soc.*, 2013, **135**, 13274–13277.
13 C.-Y. Wu, J.-W. Kang, B. Wang, H.-N. Zhu, Z.-J. Li, S.-R. Chen, L. Wang, W.-H. Yang, C. Xie and L.-B. Luo, *J. Mater. Chem. C*, 2019, **7**, 11532–11539.
14 Z. Q. Zheng, J. D. Yao and G. W. Yang, *J. Mater. Chem. C*, 2016, **4**, 8094–8103.
15 L.-B. Luo, G.-A. Wu, Y. Gao, L. Liang, C. Xie, Z.-X. Zhang, X.-W. Tong, T. Wang and F.-X. Liang, *Adv. Opt. Mater.*, 2019, **7**, 1900272.
16 Q. Zhao, W. Wang, F. Carrascoso-Plana, W. Jie, T. Wang, A. Castellanos-Gomez and R. Frisenda, *Mater. Horiz.*, 2020, **7**, 252–262.
17 C.-Y. Wu, H.-N. Zhu, M. Wang, J.-W. Kang, C. Xie, L. Wang and L.-B. Luo, *J. Mater. Chem. C*, 2020, **8**, 5375–5379.
18 S. Lee, W.-Y. Lee, B. Jang, T. Kim, J.-H. Bae, K. Cho, S. Kim and J. Jang, *IEEE Electron Device Lett.*, 2018, **39**, 47–50.
19 J.-Y. Xu, J.-S. Yu, J.-H. Liao, X.-B. Yang, C.-Y. Wu, Y. Wang, L. Wang, C. Xie and L.-B. Luo, *ACS Appl. Mater. Interfaces*, 2019, **11**, 21702–21710.
20 F.-X. Liang, J.-J. Jiang, Y.-Z. Zhao, Z.-X. Zhang, D. Wu, L.-H. Zeng, Y.-H. Tsang and L.-B. Luo, *Adv. Funct. Mater.*, 2020, **30**, 2001033.
21 Y. Shao, Z. Xiao, C. Bi, Y. Yuan and J. Huang, *Nat. Commun.*, 2014, **5**, 5784.
22 F. Wu, Q. Li, P. Wang, H. Xia, Z. Wang, Y. Wang, M. Luo, L. Chen, F. S. Chen, J. Miao, X. Chen, W. Lu, C. Shan, A. Pan, X. Wu, W. Ren, D. Jariwala and W. Hu, *Nat. Commun.*, 2019, **10**, 4663.

23 W. Li, M. J. Dai, Y. X. Hu, H. Y. Chen, X. J. Zhu, Q. X. Yang and P. A. Hu, *ACS Appl. Mater. Interfaces*, 2019, **11**, 47098–47105.
24 C. Xie, P. You, Z. Liu, L. Li and F. Yan, *Light: Sci. Appl.*, 2017, **8**, e17023.
25 C.-H. Liu, Y.-C. Chang, T. B. Norris and Z.-H. Zhong, *Nat. Nanotechnol.*, 2014, **9**, 273–278.
26 M. Peng, R. Xie, Z. Wang, P. Wang, F. Wang, H. Ge, Y. Wang, F. Zhong, P. Wu, J. Ye, Q. Li, L. Zhang, X. Ge, Y. Ye, Y. Lei, W. Jiang, Z. Hu, F. Wu, X. Zhou, J. Miao, J. Wang, H. Yan, C. Shan, J. Dai, C. Chen, X. Chen, W. Lu and W. Hu, *Sci. Adv.*, 2021, **7**, eabf7358.
27 L. Tong, X. Huang, P. Wang, L. Ye, M. Peng, L. An, Q. Sun, Y. Zhang, G. Yang, Z. Li, F. Zhong, F. Wang, Y. Wang, M. Motlag, W. Wu, G. J. Cheng and W. Hu, *Nat. Commun.*, 2020, **11**, 2308.
28 C. M. Lochner, Y. Khan, A. Pierre and A. C. Arias, *Nat. Commun.*, 2014, **5**, 5745.
29 J. Huang, J. Lee, J. Vollbrecht, V. V. Brus, A. L. Dixon, D. X. Cao, Z. Zhu, Z. Du, H. Wang, K. Cho, G. C. Bazan and T.-Q. Nguyen, *Adv. Mater.*, 2019, **32**, 1906027.
30 M. Elgendi, *Curr. Cardiol. Rev.*, 2013, **8**, 14–25.

